# Supplementary material
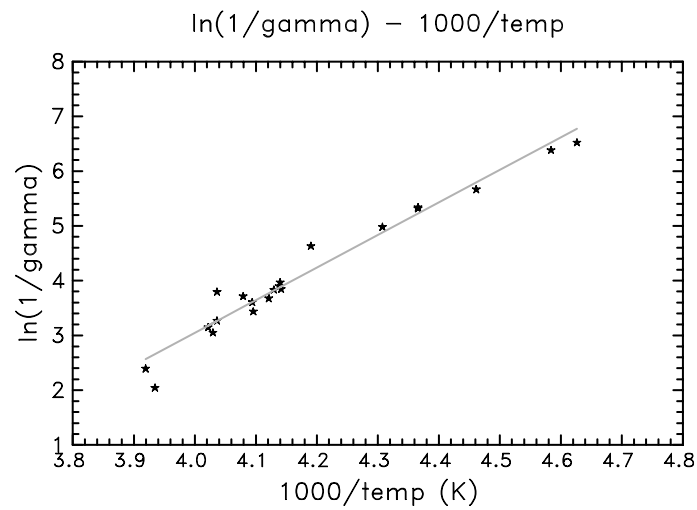


*Supplementary Figure S1*: *Logarithmic representation of γ coefficient in Equation (4) as a function of the site temperature. The stars represent the γ coefficient calculated by the model for each site, the grey line represents a linear regression. Its slope allows evaluation of the activation energy relative to the snow densification mechanism in the model: 49.5 kJ/mol.*
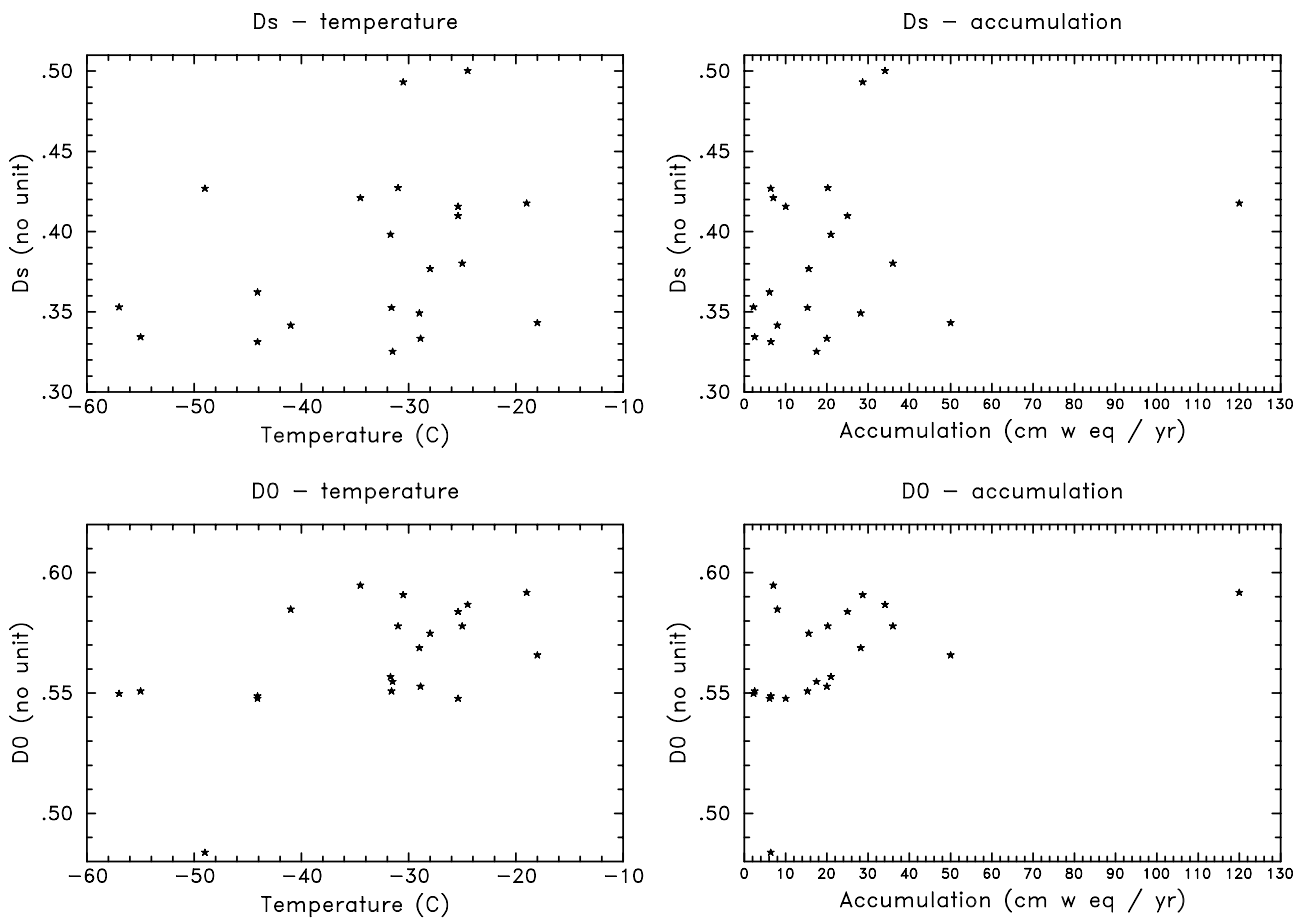
*Supplementary Figure S2*: *Variations of the surface (Ds) and critical (D0) relative densities with site temperature and accumulation. Ds is the value of the polynomial fit to density data represented on Figures S3 and S7 at the surface. D0 is adjusted to minimize the root mean square deviations between model results and the polynomial fit to density data between the surface and the depth at which a density of 840 kg/m³ is reached. No correlation between Ds or D0 with temperature or accumulation could be found. Although the variability of Ds and D0 are large, their impact on the LID is relatively small as illustrated on Figure S3.*



Km 105 (−24.5C, 34.1cm)
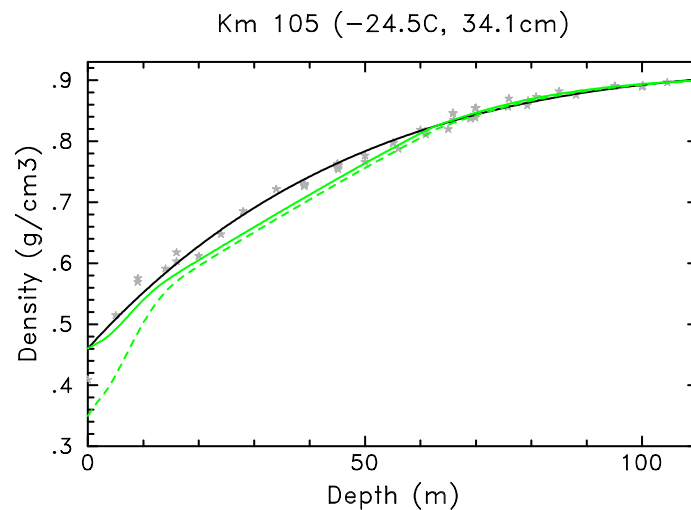
*Supplementary Figure S3*: *Impact of the surface density value (Ds) on model results at Km 105 site. Grey stars represent measured densities, the black line represents a polynomial fit to density data. The two green curves represent model results obtained with two largely different values of the surface density. Lower values of Ds lead to faster modelled densification rates. While the difference between the two densification curves is important at the surface, the two curves are almost similar in the deep firn. The difference on Ds thus does not have much importance for the determination of the LID.*



Equivalent Activation Energy
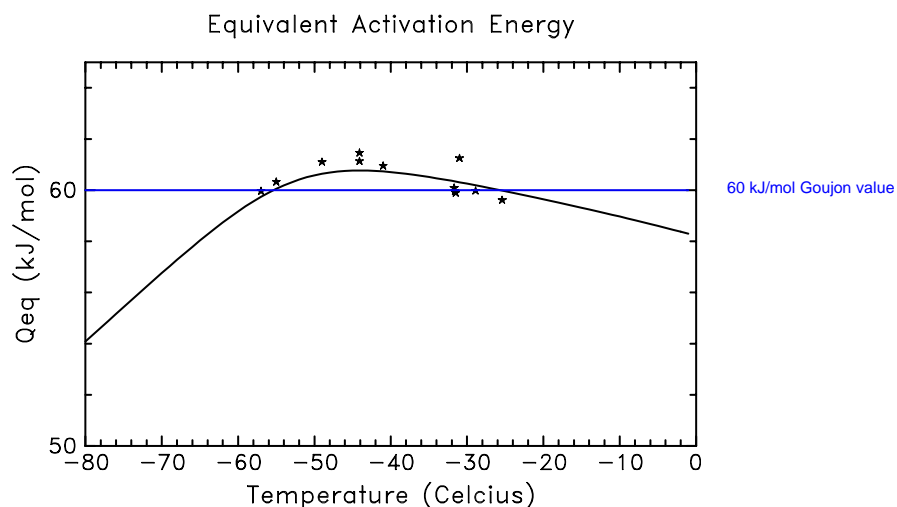
_Supplementary Figure S4_: Equivalent activation energies calculated for our model (without impurity effect, black line; with impurity effect for present day sites with available calcium concentrations, black stars).The blue line represents the value of 60kJ/mol used in Goujon et al. (2003).

For our model, the equivalent activation energy $Q_{eq}$ is calculated by solving: $e^{\frac{-Q_{eq}}{RT}} = a_1 \times e^{\frac{-Q_1}{RT}} + a_2 \times e^{\frac{-Q_2}{RT}} + a_3 \times e^{\frac{-Q_3}{RT}}$ .
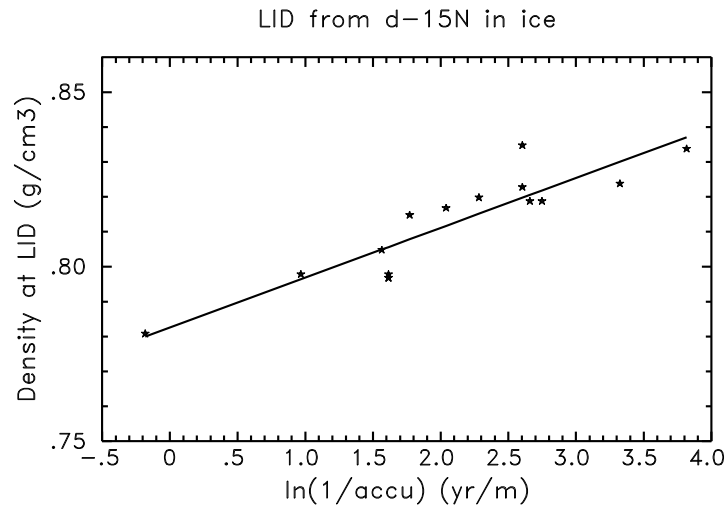


_Supplementary Figure S5_: Calculated density at LID with the Witrant et al. (2012) model of gas transport in firn (see main text, Section 2.4) as a function of the logarithm of the inverse of the accumulation rate (in m w. eq./yr). The stars show the results at individual firn air pumping sites (12 sites, 15 boreholes), and the line shows the regression presented in Equation (10) of the main text. The correlation coefficient is 0.9.
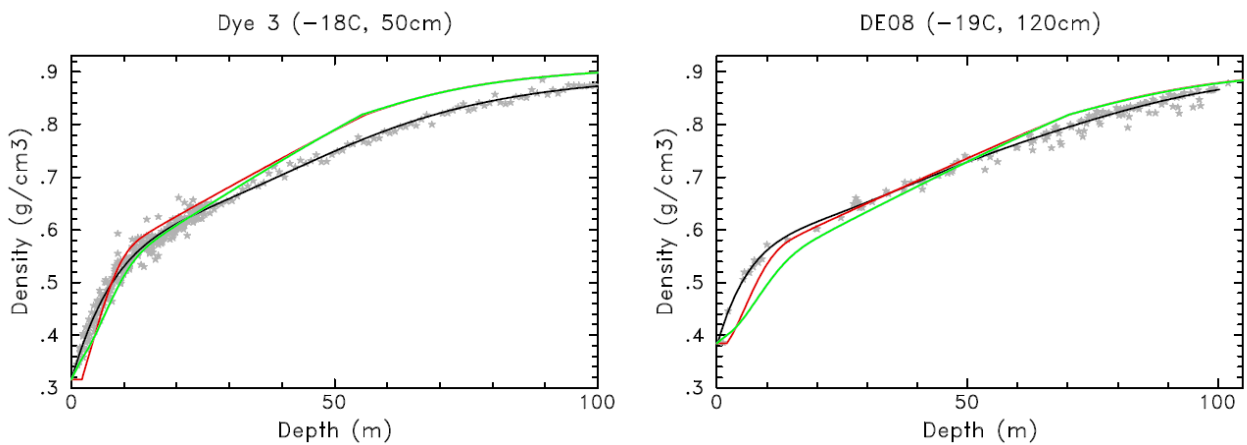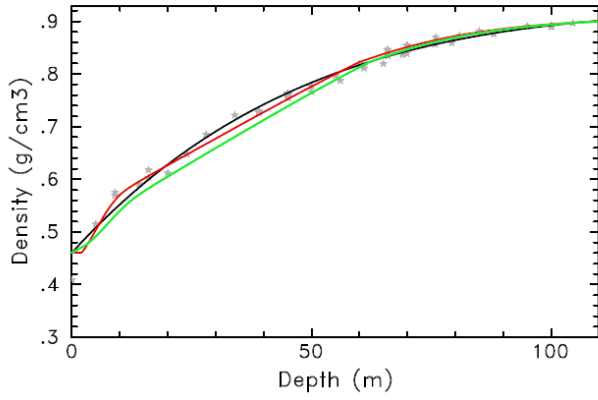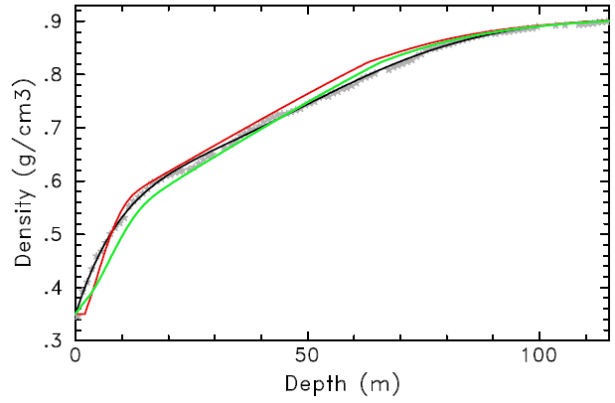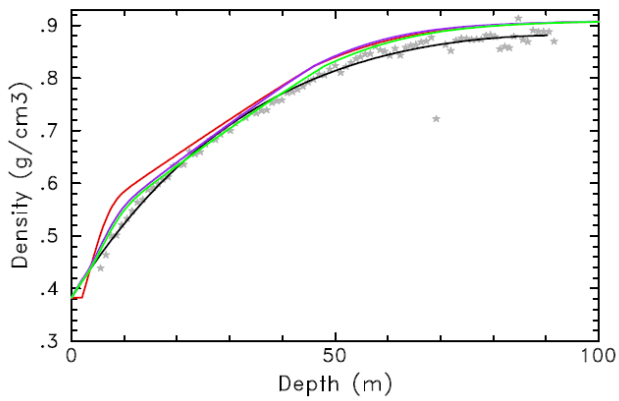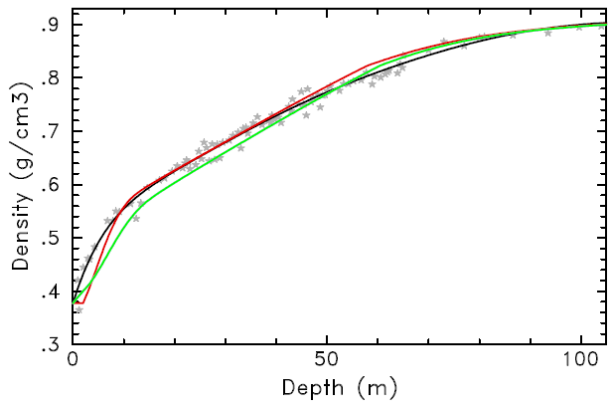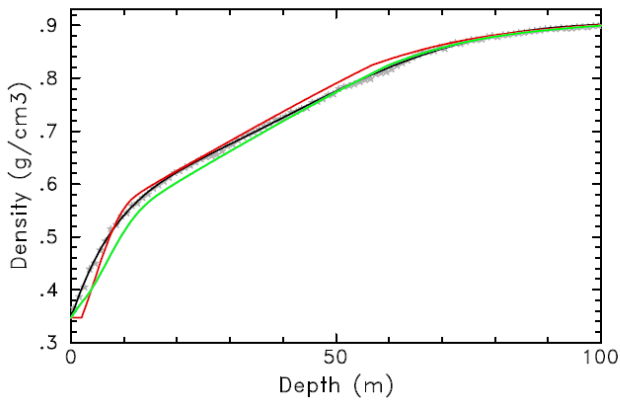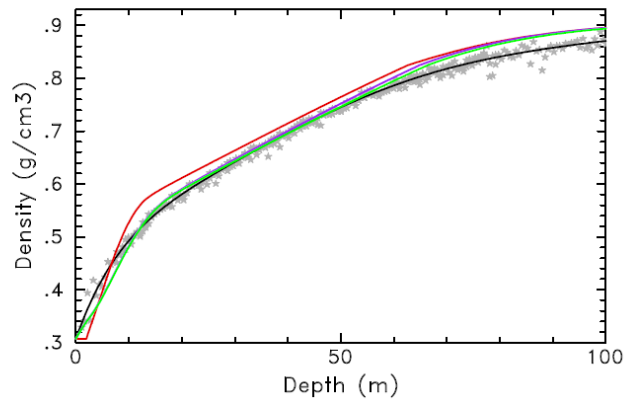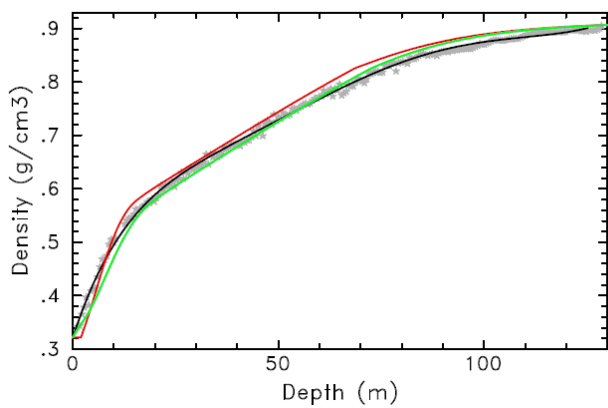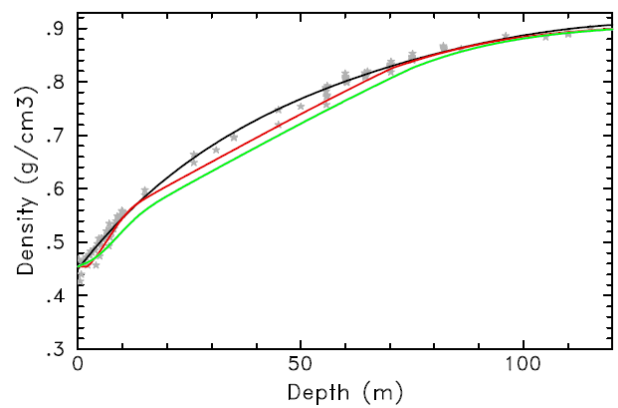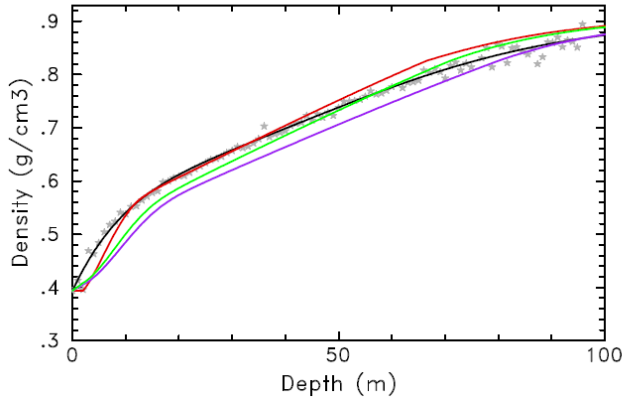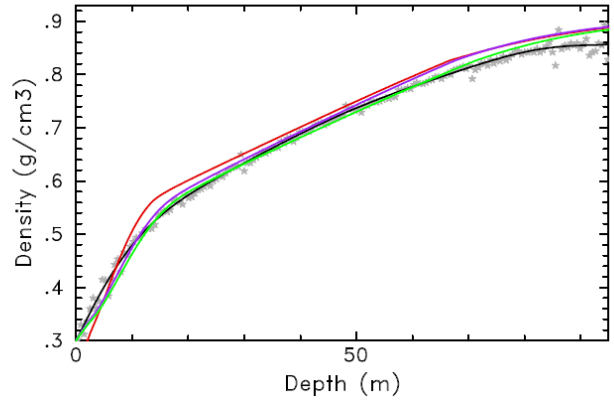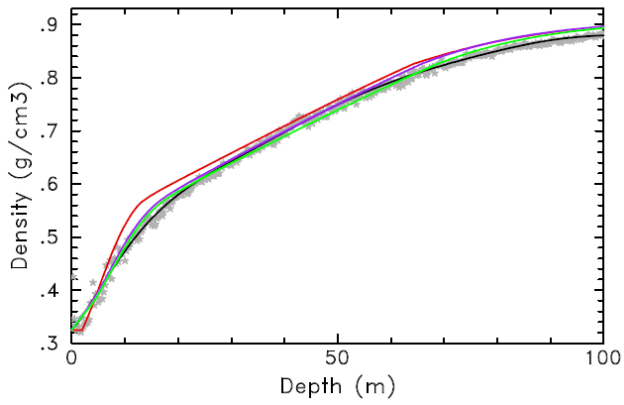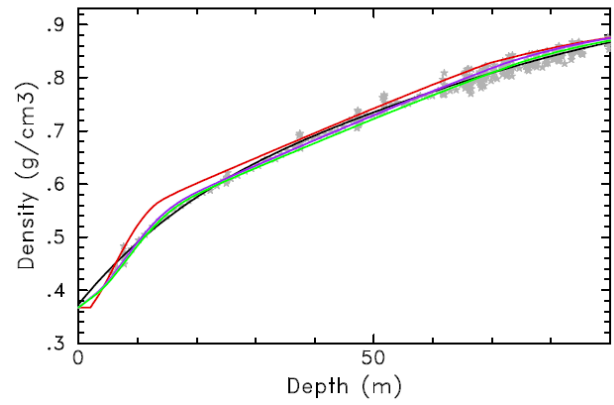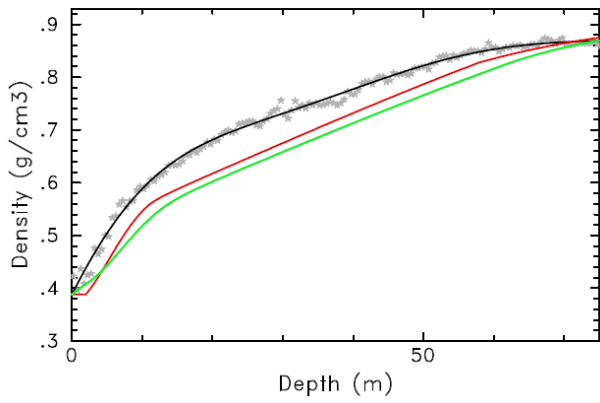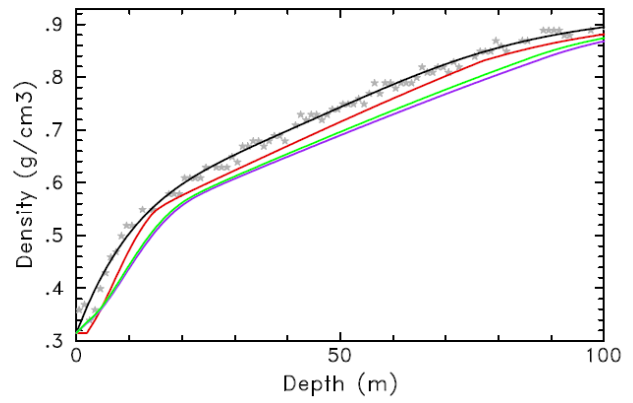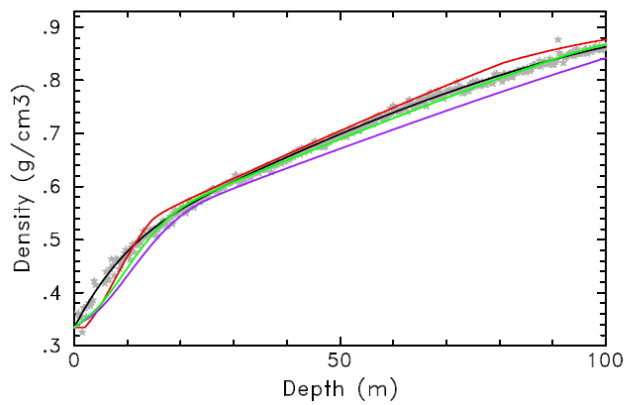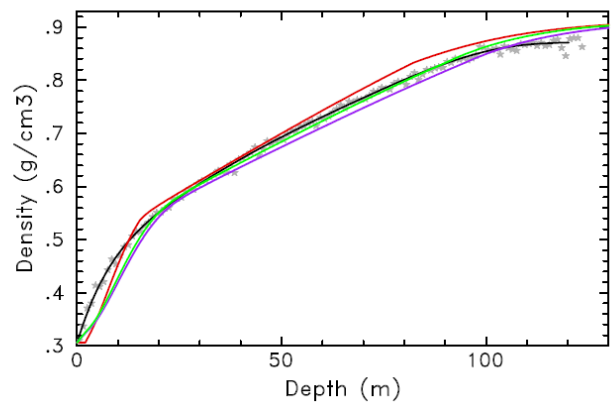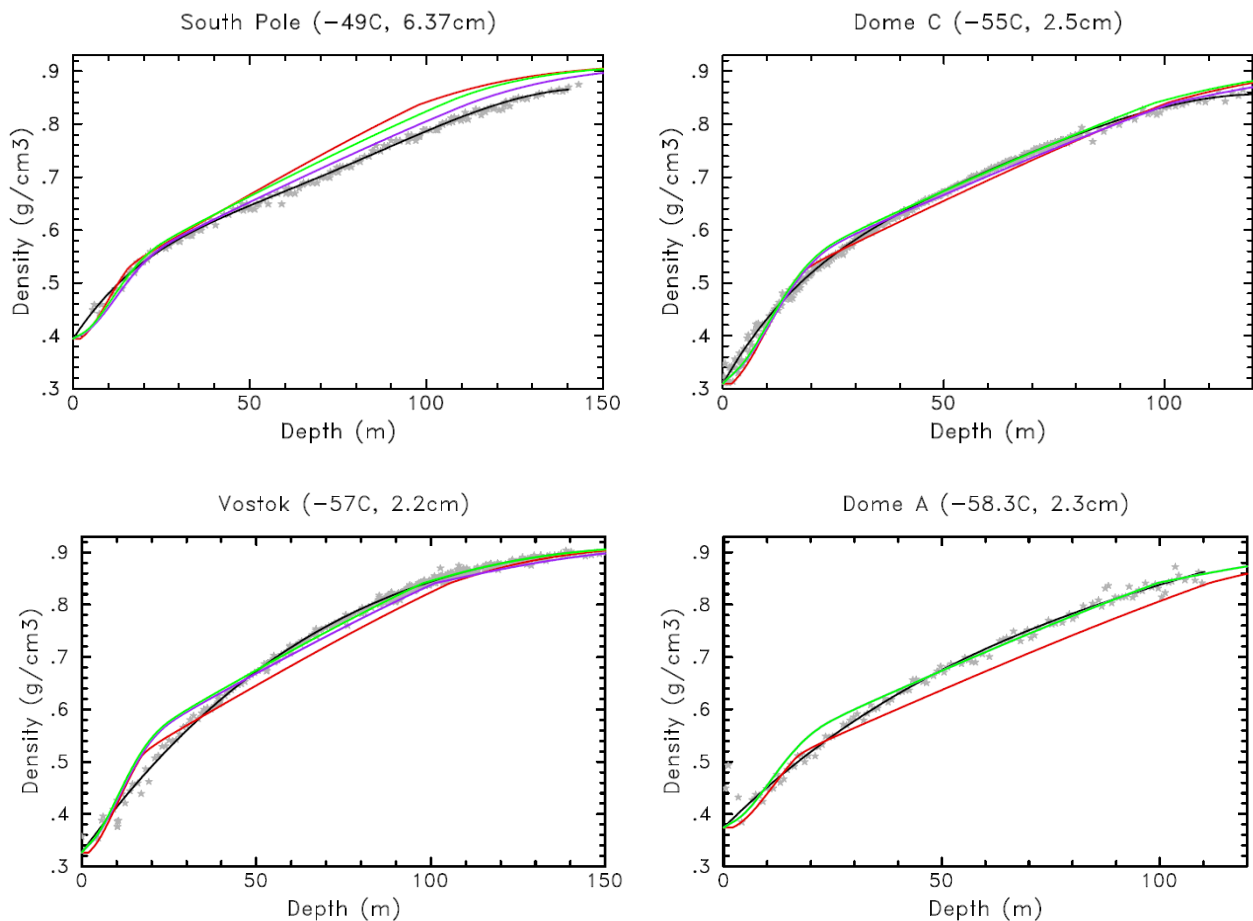
*Supplementary Figures S6: Measured and modelled density profiles for 22 sites, the grey stars correspond to the data, the polynomial fit to the data is in black, the density profile simulated with the old version of the LGGE model is in red, the density profile simulated with the new version of the LGGE model is in green and the density profile simulated with the new version of the LGGE model with the dust effect in purple.*
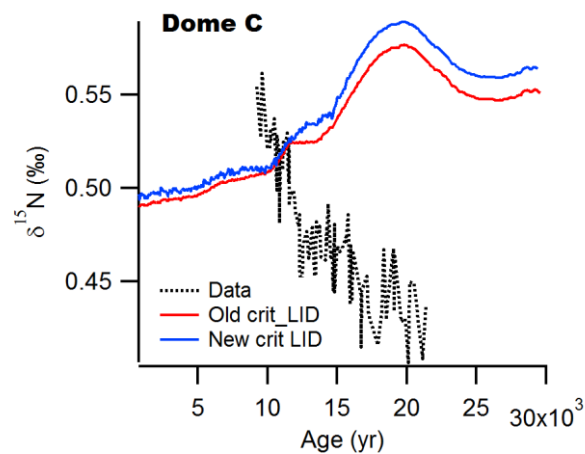


*Supplementary Figure S7: Comparison of the measured (in black) and the old modelled $\delta^{15}N$ at Dome C. The simulated $\delta^{15}N$ using the old gas trapping criterion is in red and the simulated $\delta^{15}N$ using the new gas trapping criterion is in blue.*
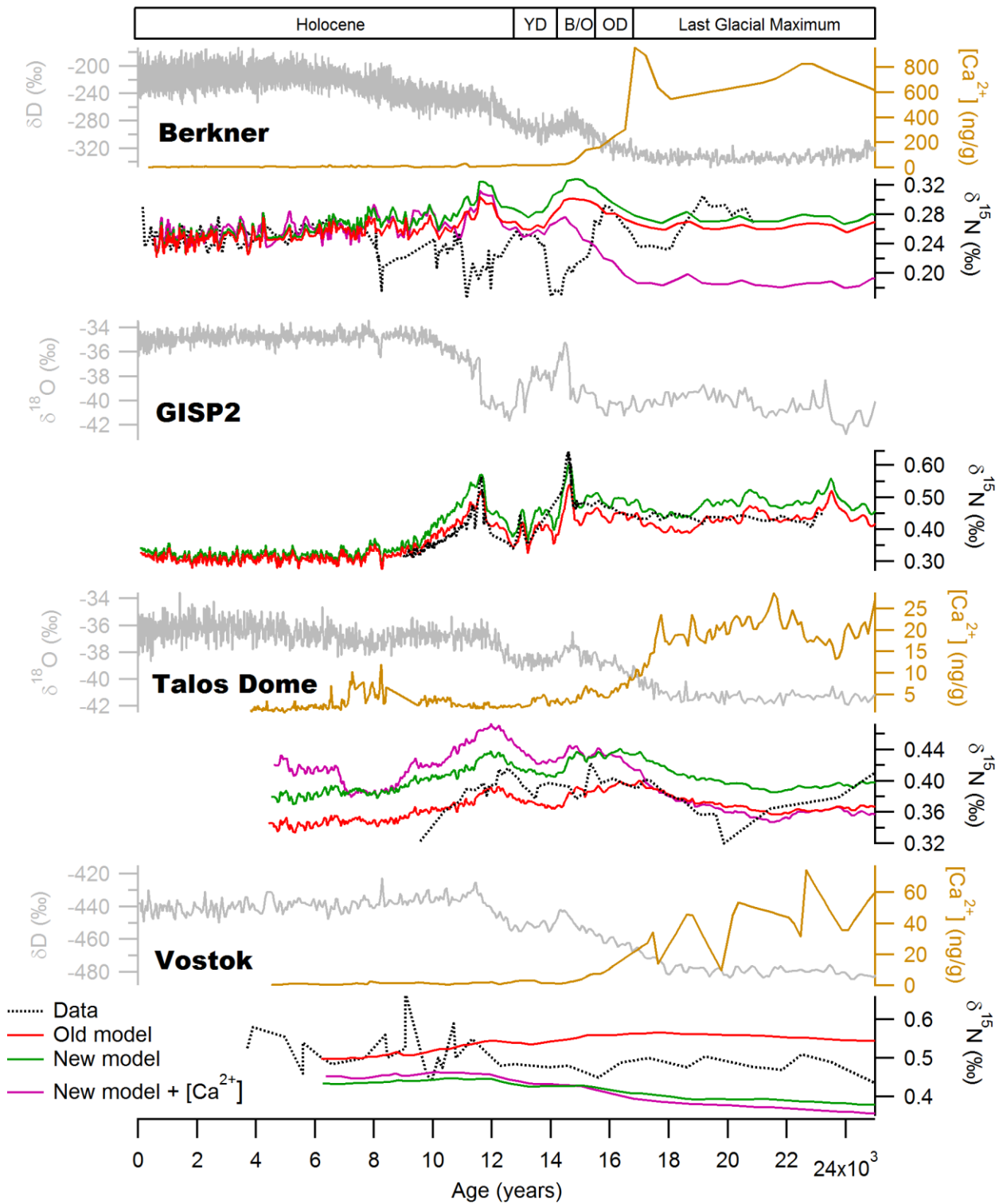
_Supplementary Figure S8:_ _Comparison of the measured_ δ¹⁵N _(black) and the modeled_ δ¹⁵N _(old (red), new version (green) and new version with impurity (purple)) of the LGGE model for Berkner, GISP2, Talos Dome and Vostok. The water δ¹⁸O or δD profiles are displayed in grey and the calcium concentration profile in gold._
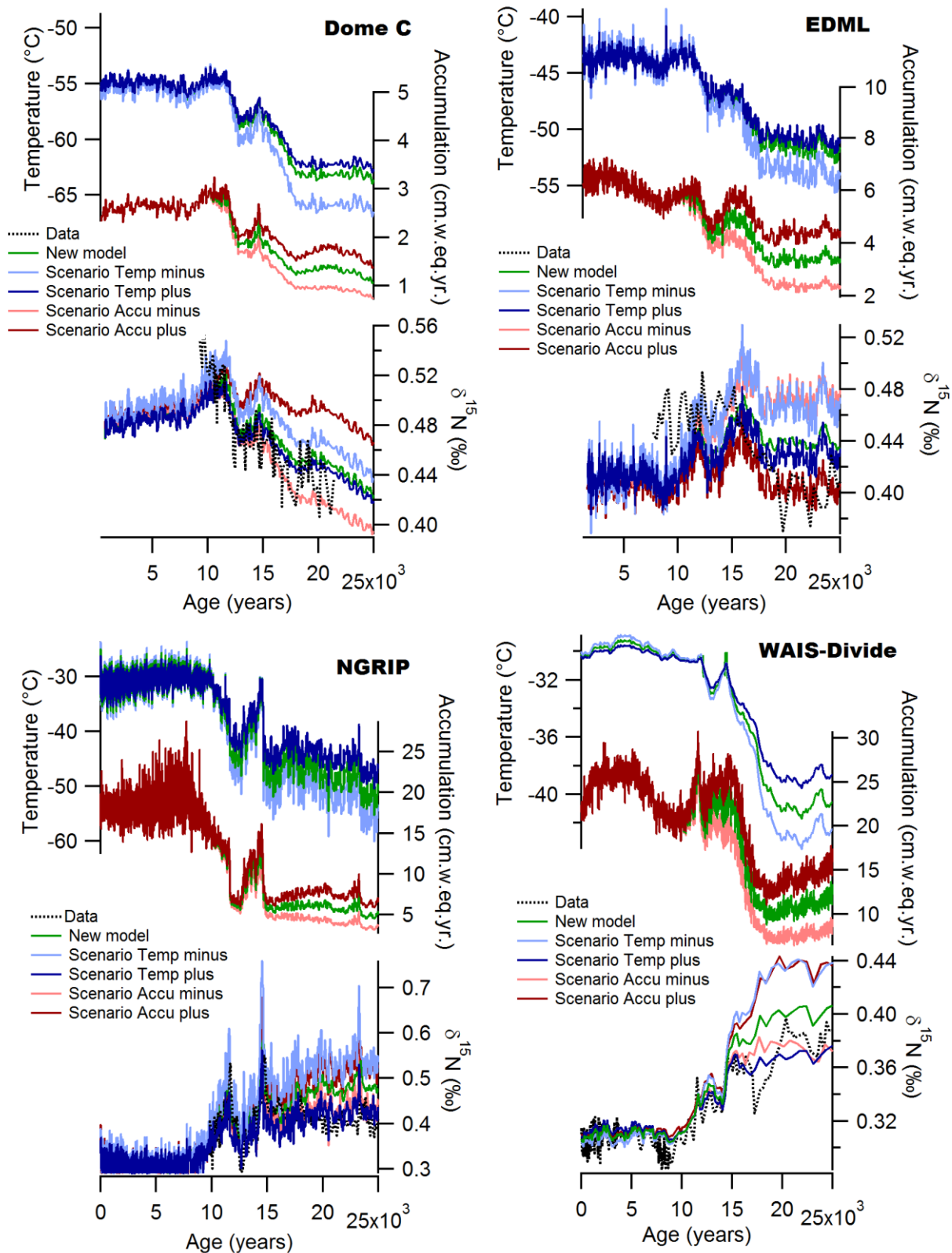
*Supplementary Figure S9: Comparison of the measured (black) and modelled $\delta^{15}N$ at Dome C, EDML, NGRIP and WAIS-Divide over the last deglaciation with our new model without impurity effect, using five different temperature and accumulation rate scenarios. The standard scenarios (Table S2) and corresponding $\delta^{15}N$ model outputs are in green. For building the Accu minus/plus and Temp minus/plus scenarios displayed on the two upper panels for each sites, we took the uncertainties mentioned in the main text: Accu minus*

*correspond to a LGM accumulation rate of -30% (-20%) in Antarctica (Greenland) compared to the standard run; Accu plus corresponds to a LGM accumulation rate of +30% (+20%) in Antarctica (Greenland) compared to the standard run. In Antarctica, Temp plus corresponds to a decrease by 10% of the temperature increase over the last deglaciation (i.e. warmer LGM temperature); Temp minus corresponds to an increase by 30% of the temperature increase over the last deglaciation (i.e. lower LGM temperature).  In Greenland, Temp minus and Temp plus are scenarios were the temperature of the LGM is changed by +3 and -3°C.*

*Within the uncertainty range of the model inputs, it is possible to match the measured δ$^{15}$N with the model except for EDML where the modelled δ$^{15}$N LGM to EH change is always too small even with the scenario Accu plus. Note that the same figures can be obtained with the old version of the LGGE model with similar amplitude for the differences in simulated LGM δ$^{15}$N level between the different scenarios.*
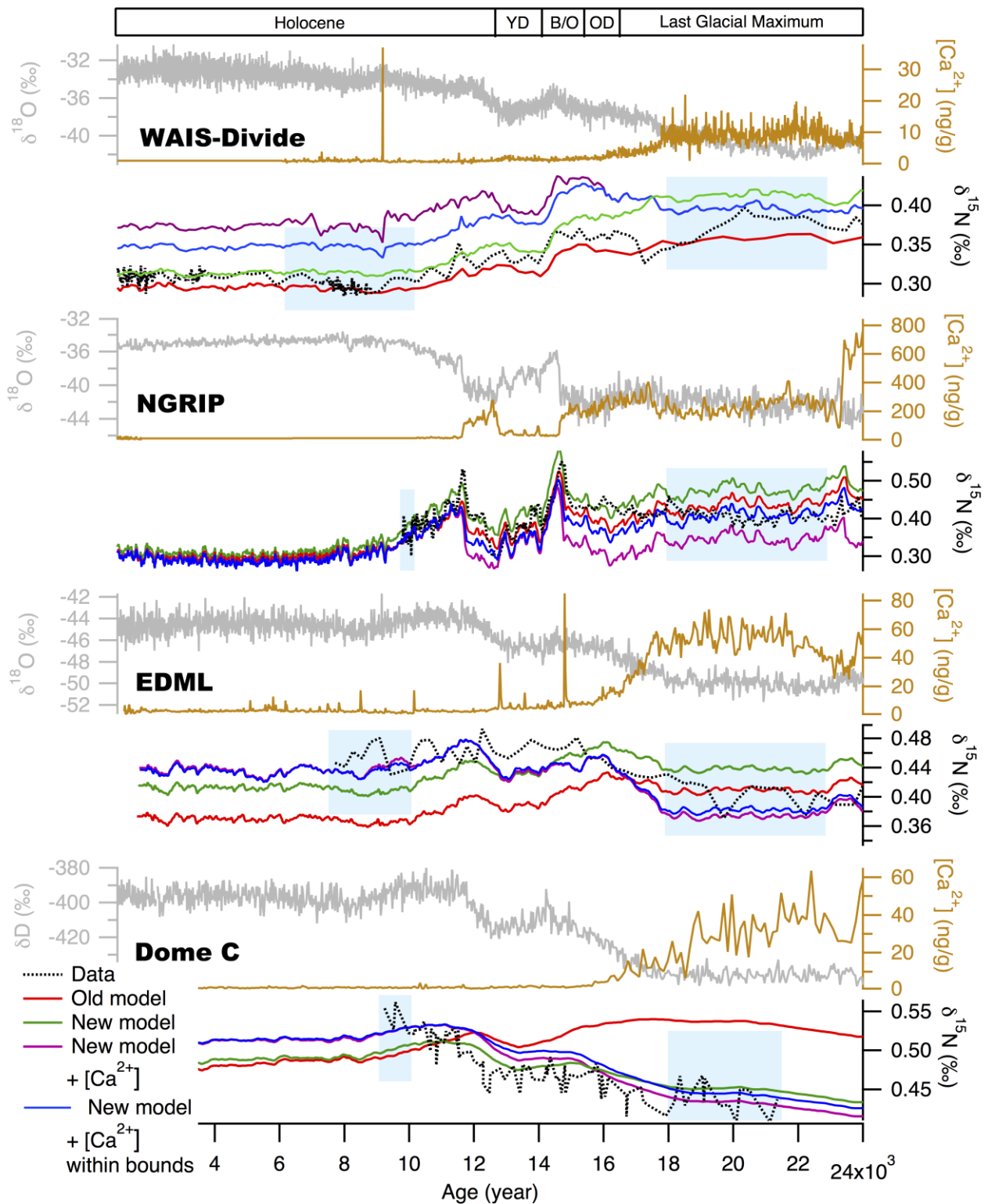
*Supplementary Figure S10*: *Comparison of the measured δ¹⁸O or δD (grey), the calcium concentration (gold), the measured δ¹⁵N (black) and the modelled δ¹⁵N (old (red), new version (green), new version with impurity following Freitag parameterization (purple) and new version with impurity (blue) using a parameterization with threshold for high and low values of the calcium concentration) of the LGGE model for WAIS-Divide, NGRIP, EDML and Dome C. Blue boxes for each sites indicate the periods over which the d¹⁵N average for the LGM and EH have been estimated for the calculation of the amplitude of the d¹⁵N change over the deglaciation*

| Sites | Location (Latitude ; Longitude) | Temperature (°C) | Accumulation (cm.w.eq.yr) | $[Ca^{2+}]$ (ng/g) | Surface density (kg/m³) | $\sigma_{fit\text{-}data}$ (kg/m³) | $\sigma_{old\ model\text{-}fit}$ (kg/m³) | $\sigma_{new\ model\text{-}fit}$ (kg/m³) | $\sigma_{new\ model\ with\ dust\text{-}fit}$ (kg/m³) |
|---|---|---|---|---|---|---|---|---|---|
| Dye 3 [1] | 65°11'N ; 43°50'W | -18.0 | 50.0 | X | 357 | 13.8 | 32.7 | **30.8** | X |
| DE08 [2] | 66°43'19"S ; 113°11'58"E | -19.0 | 120.0 | X | 384.2 | 10.3 | **20.9** | 29.8 | X |
| Km105 [4] | 67°58'S ; 93°70'E | -24.5 | 34.1 | X | 460.5 | 14.0 | **10.7** | 21.1 | X |
| Site 2 [5] | 76°59'N ; 56°04'W | -25.0 | 36.0 | X | 350.1 | 5.8 | **18.3** | 19.2 | X |
| Siple Dome [3] | 81°39'3"S ; 148°47'66"W | -25.4 | 10.0 | 8.0 | 382.7 | 8.9 | 29.4 | **13.2** | 19.5 |
| D-47 [6] | 67°23'S ; 138°43'E | -25.4 | 25.0 | X | 377.4 | 12.5 | **15.9** | 21.8 | X |
| Byrd [7] | 80°S ; 120°W | -28.0 | 15.6 | X | 347.1 | 3.8 | **15.9** | 18.6 | X |
| NEEM [8] | 77.45°N ; 51.06°W | -28.9 | 20.0 | 7.4 | 307.2 | 8.0 | 27.2 | **13.5** | 15.8 |
| Crête (site A) [9] | 70°38'5.68"N ; 324°10'48"E | -29.0 | 28.2 | X | 321.7 | 7.0 | 18.7 | **14.0** | X |
| Km200 [10] | 68°15'S ; 94°05'E | -30.5 | 28.7 | X | 454.4 | 10.5 | **21.8** | 37.7 | X |
| WAIS divide [11] | 79°28'S ; 112°05'W | -31.0 | 20.2 | 1.58 | 393.7 | 8.7 | **18.2** | 21.3 | 35.1 |
| Ngrip [12] | 75°10'N ; 42°32'W | -31.2 | 17.5 | 10.0 | 299.9 | 6.9 | 22.2 | **9.9** | 13.4 |
| Grip [13] | 72°34'N ; 37°37'W | -31.7 | 21.0 | 7.8 | 367.0 | 6.7 | 18.9 | 10.3 | **8.8** |
| B29 [14] | 76°00'N ; 43°29'E | -31.6 | 15.3 | 9.2 | 325 | 10.1 | 22.7 | **7.2** | 10.2 |
| Mizuho [15] | 70°41'53"S ; 44°19'54"E | -34.5 | 7.0 | X | 421 | 9.8 | **50.0** | 66.5 | X |
| Talos Dome [16] | 72°49'S ; 159°11'E | -41.0 | 8.0 | 4.0 | 315.3 | 12.1 | **29.6** | 46.0 | 51.9 |
| B32 [17] | 75°00'S ; 0°00'E | -44.1 | 6.1 | 1.7 | 334.5 | 6.2 | 15.6 | **13.3** | 28.7 |
| EDML [18] | 75°S ; 0'04°E | -44.1 | 6.4 | 3.0 | 305.9 | 5.3 | 19.4 | **16.9** | 23.6 |
| South Pole [19] | 90°S | -49.0 | 6.37 | 2.0 | 394.4 | 6.4 | 35.5 | 26.7 | **15.2** |
| Dôme C [20] | 75°06'S ; 123°21'E | -55.0 | 2.5 | 1.8 | 309.2 | 6.2 | 15.3 | **11.0** | **11.0** |
| Vostok [21] | 78°28'S ; 106°48'E | -57.0 | 2.2 | 1.6 | 326.5 | 8.0 | 28.0 | 23.5 | **23.0** |
| Dome A [22] | 80°22'01.6"S ; 77°22'22.3E | -58.3 | 2.3 | X | 374 | 9.8 | 32 | **13.4** | X |

References below were used for the following data: [a] location, [b] density, [c] temperature, [d] accumulation, [e] calcium concentration

Best efforts were made to find information about the methodologies used for density measurements. The following Greek letters are used to indicate the method used, the use of several letters for the same site implies that several data series were used.

α: volume and weight measurements on whole cores or bags. The precision of such measurements is dependent on the regularity of the core shape.

β: volume and weight measurements in firn, and high precision hydrostatic weighing measurements in ice

γ: volume and weight measurements on machined samples (regular volume, samples are often small)

δ: gamma ray beam attenuation through the ice core (very high resolution)

ε: camera assisted volume measurements, and weight measurements (high resolution)

[1] [a, c, d] Robin, 1983; [b] http://gcmd.nasa.gov/r/d/LSSU_and PSU_Firn_data Spencer et al., 2001

[2] [a, b, c, d] Etheridge and Wookey, 1989; [b] Arnaud et al., 1998, 2000, γ density measurement method

[3] [a, b] https: //nsidc.org/data/waiscores/corec.html, [c] Butler et al., 1999; Jones et al., 2014; Kreutz et al., 1999, 2000, α density measurement method

[4] [a, b, c, d] Salamatin et al., 2009, γ density measurement method

[5] [a, c,] Robin, 1983; [b] http://gcmd.nasa.gov/r/d/LSSU_PSU_Firn_data Spencer et al., 2001 originally from Langway, 1967 with β density measurement method

[6] [a, b, c, d] Arnaud et al., 1998 with β density measurement method

[7] [a, b, c, d] http://gcmd.nasa.gov/r/d/LSSU_PSU_Firn_data Spencer et al., 2001, originally from Gow, 1968 with β density measurement method

[8] [a, b, c] Buizert et al., 2012; [b] Steen-Larsen et al., 2011 ; [e] Gfeller et al., 2014, α density measurement method

[9] [a, b, c, d] http://gcmd.nasa.gov/r/d/LSSU_PSU_Firn_data and Spencer et al., 2001 ; [b] originally from Clausen et al., 1988

[10] [a, b, c, d] Salamatin et al., 2009; [b] Arnaud et al., 1998, γ density measurement method

[11] [a, b, c, d] Fitzpatrick et al., 2014 ; [e] Cole-Dai et al., 2013

[12] [a, c, d] Ngrip community members, 2004, [b] H.C. Steen-Larsen Pers. Comm., [e] Svensson pers. Comm., 2016, α density measurement method

[13] [a, b, c, d] http://gcmd.nasa.gov/r/d/LSSU_PSU_Firn_data and Schwander et al., 1997; [e] Iizuka et al., 2008, α and γ density measurement methods

[14] Freitag et al., 2013; Hörhold et al., 2011, δ density measurement method

[15] [a, c, d] (Nishio et al., 1979) ; [b] (Narita and Maeno, 1978), γ density measurement method

[16] [a, c] www.taldice.org/project/site ; [b] www.taldice.org/data (data from F. Parrenin) ; [d] Stenni et al., 2002 [e] Schüpbach et al., 2013

[17] Freitag et al., 2013; Hörhold et al., 2011, δ density measurement method

[18] [a, b] Kipfstuhl et al., 2009 ; [c] Freitag et al., 2013; [d] Oerter et al., 2004; [e] Fischer et al., 2007, α density measurement method

[19] [a, b, c] http://gcmd.nasa.gov/r/d/LSSU_PSU_Firn_data and Spencer et al., 2001 ; [d] Mosley-Thompson et al., 1995; [e] Ferris et al., 2011

[20] [a, d] Gautier et al., 2016, [b] R. Mulvaney pers. com. and Leduc-Leballeur et al., 2015; [c] Arnaud et al., 2000 ; [e] Lambert et al., 2012, α and ε density measurement methods

[21] [a, c, d] Arnaud et al., 2000 ; [b] http://gcmd.nasa.gov/r/d/LSSU_PSU_Firn_data and Spencer et al., 2001 and J.-M. Barnola, unpublished (using γ density measurement method); [e] De Angelis et al., 1997

[22] [a, b, c] Cunde et al., 2008 ; Cunde pers. com. 2016 ; d: Hou et al., 2007 and Ding et al., 2016, α density measurement method

*Supplementary Table S1: Standard deviation between modeled and measured density profiles for 22 polar sites, for the old LGGE model and the new LGGE model*

*(with three different activation energies in the firn densification module noted "new model" and with three different activation energies depending on Ca$^{2+}$ concentration in the firn densification module noted "new model with dust"). The values in bold indicate the lowest standard deviation between modeled and fitted density profiles for each site.*

| Δage | Data | Old | New | New + dust |
|------|------|-----|-----|------------|
| Dye 3 | 78 | **68.4** | 61.8 | - |
| DE08 | 35.5 | **36.8** | 31.3 | - |
| km105 | 104.4 | 111.7 | **106.4** | - |
| Site2 | 112.2 | **109.2** | 103.3 | - |
| Siple Dome | 329 | 287.9 | **296.9** | 284.9 |
| D-47 | 152 | **145.3** | 141.7 | - |
| Byrd | 238.9 | 225 | **226.9** | - |
| NEEM | 209.4 | 187.4 | **191.9** | 187.4 |
| Crete | 156.1 | **150** | 145.7 | - |
| km200 | 137.9 | 156.7 | **152.6** | - |
| WAIS divide | 225 | 206.5 | 206.5 | **233.3** |
| North GRIP | 248.4 | 226.2 | **236.5** | 224.5 |
| GRIP | 209.9 | **205.7** | **205.7** | 200 |
| B29 | 270.3 | 251 | **264.7** | 252.9 |
| Mizuho | 483.7 | **518.4** | 557 | - |
| Talos | 554.1 | **592.6** | 637.7 | 656.4 |
| B32 | 896.8 | 816.1 | **889.9** | 978.4 |
| EDML | 874.5 | 787.3 | **852.9** | 899.7 |
| SP | 1160.9 | 965.2 | 1002.8 | **1068.7** |
| DC | 2639.1 | 2473 | 2461 | **2557** |
| Vostok | 2814.3 | 2960.4 | **2810.4** | 2919.5 |
| Dome A | 2812.7 | 3024.8 | **2764** | - |

Supplementary Table S2: Comparison of Δage at the bottom of the firn for the different sites studied here. The main features already observed for the comparison of the standard deviation between modeled and measured density profiles (Table S1) are also observed here. This is the case for the worsened agreement between model and data at Talos and Mizuho when using the new parameterization or the improved model vs data agreement at low temperature and low accumulation sites of the bottom of the table (B32, EDML, South Pole, Dome C, Vostok, Dome A).

| Sites | Temperature scenario | Accumulation rate scenario | Calcium scenario |
|---|---|---|---|
| NGRIP | Dahl-Jensen et al., 1998 ; Kindler et al., 2014 | Bazin et al., 2013 | Svensson (comm. pers.) and Seierstad et al., 2014 |
| Dome C | Stenni et al., 2010 | Bazin et al., 2013 | Fischer et al., 2007 and Lambert et al., 2012 |
| EDML | Stenni et al., 2010 | Bazin et al., 2013 | Fischer et al., 2007 |
| WAIS-Divide | Buizert et al., 2015 and WAIS Divide Project Members, 2013 | Fudge et al., 2016 | Buizert et al., 2015 |
| Berkner Island | Capron et al., 2013 | Capron et al., 2013 | Capron et al., 2013 |
| GISP2 | Cuffey and Clow, 1997 | Cuffey and Clow 1997 | X |
| Talos Dome | Buiron et al., 2011 | Bazin et al., 2013 | Schüpbach et al., 2013 |
| Vostok | Cuffey and Vimeux, 2001 | Bazin et al., 2013 | Legrand et al., 1988 |

*Supplementary Table S3: References of the temperature, accumulation rate and calcium scenarios over the last deglaciation for NGRIP, Dome C, EDML, WAIS-Divide, Berkner Island, GISP2, Talos Dome and Vostok. The temperature (T) scenario for NGRIP has been built so that its temporal evolution reflects the $\delta^{18}O$ temporal evolution (T=a$\delta^{18}O$+b) with an adjustment of a and b to reflect the ~ 20°C temperature change between LGM and Holocene (Dahl-Jensen et al., 1998) as well as abrupt change of temperature of ~12.5°C and ~10.5°C at the onset of the Bølling-Allerød and end of Younger Dryas as given by Kindler et al. (2014)*

| EH – LGM (‰) | Dome C | EDML | NGRIP | WAIS-D |
|---|---|---|---|---|
| Measured | 0.1051 | 0.0538 | -0.0986 | -0.0780 |
| Old | -0.0404 | -0.0446 | -0.1080 | -0.0639 |
| Old + dust | 0.0904 | 0.0545 | -0.0088 | -0.0078 |
| New parameterization (Table 1) | 0.0519 | -0.0313 | -0.112 | -0.0909 |
| New parameterization + dust | 0.0930 | 0.0651 | -0.00937 | -0.0129 |
| Test A | -0.0183 | -0.0331 | -0.0842 | -0.0648 |
| Test A + dust | 0.0714 | 0.0474 | -0.00282 | -0.00658 |
| Test B | -0.0336 | -0.0644 | -0.147 | -0.10 |
| Test B + dust | 0.106 | 0.0604 | -0.0272 | -0.0225 |
| New parameterization + dust following Freitag parameterization for the Pimienta – Barnola model | 0.0915 | 0.0646 | -0.00717 | -0.0092 |

*Supplementary Table S4: Results of the difference between the average of the Early Holocene (EH) and the average of the Last Glacial Maximum (LGM) for the sensitivity tests displayed on Figure 7 for the 4 sites described in the main text.*

| NGRIP | Δage (old version) | Δage (new version) | Δage (new version + dust) | DATA |
|---|---|---|---|---|
| Bølling /Allerød | 870 years | 920 years | 740 years | 1058±100 years |
| End of Younger Dryas | 760 years | 820 years | 640 years | 819±100 years |

*Supplementary Table S5: Comparison of measured and modelled Δage with different parameterizations of the model at two different points of the last deglaciation at NGRIP. The only way to compare Δage model output with data is actually on the abrupt warming recorded very clearly both in the $\delta^{18}O$ in the ice phase and $\delta^{15}N$ in the gas phase on the NGRIP ice core because we have an accurate associated timescale (GICC05). The "data" values for the Δage have been deduced from the identification of the peak of the $\delta^{15}N$ and mid-slopes of $\delta^{18}O_{ice}$ increases recording the most abrupt warming phases of the last deglaciation associated with the Bølling-Allerød and the end of the Younger Dryas. The $\delta^{15}N$ record is given in Kindler et al. (2014) and the $\delta^{18}O_{ice}$ record is given in NGRIP comm members (2004). The respective depths for $\delta^{15}N$ peaks are 1629.4 and 1515.3 m. The respective depths for the $\delta^{18}O_{ice}$ mid-slopes are 1604.2 and 1491.5 m . We obtained the Δage indicated in the Table S2 when translating these depth differences in age through the use of the GICC05 age scale. The agreement between data and model is slightly better when using the new version but the addition of dust leads to a strong deterioration as observed on the $\delta^{15}N$ profiles.*
*NB: the uncertainty on the Δage from the data is mainly linked to the resolution of the $\delta^{15}N$ signal.*

*Supplementary Text S1: Model input files and running conditions*


For paleoclimate applications, we have one input file for each site. The file has 5 columns: depth, age, difference of temperature with respect to present-day surface temperature, accumulation rate and calcium concentration. Except for WAIS-D, the spatial resolution is constant from the top to the bottom of each ice core and varies between sites between 1 and 2 m. Such resolution is largely sufficient to depict the temporal variability of temperature and accumulation over the last deglaciation (the lowest temporal resolution is 200 years at Vostok for the LGM; at NGRIP, the temporal resolution corresponding to 1 m spatial resolution in the input file is about 50 years at LGM). For WAIS-D, the input files were designed so that the temporal resolution is constant to 10 years all along the ice core.

The model running conditions are very similar to those described in Goujon et al. (2003). For density calculation, the depth step is 0.25 m down to 150 m depth, 2.5 m depth down to 550 m depth and 25 m depth below. We only simplified the boundary between the 2.5 m and 25 m grids to guarantee that the change occurs at a grid node (Goujon et al. (2003) used a criterion based on the difference between pure ice density and the modelled density). Relative coordinates z/H (H being the ice thickness) are used for solving the ice sheet vertical velocity equation as in Goujon et al. (2003).

In this study, we modified the time step: Goujon et al. (2003) used a one year time step for all sites, whereas we adjusted the time step in link with the maximum accumulation rate in the input file. Indeed the accumulation rate defines the firn sinking speed. Stable results are obtained with a time step of $0.3/\max(Ac)$ where Ac is the accumulation rate in m w.eq.$yr^{-1}$. Thus our time step is shorter than one year only at very high accumulation rate sites (Ac > 0.3m w.eq./yr). Numerical tests showed that with the above depth and time grid, Eulerian and Lagrangian calculations of the density profiles lead to consistent results. However, for gas age calculations, a lagrangian tracking of firn layers is necessary to simulate the detailed shape of $\delta^{15}N$ anomalies during Dansgaard-Oeschger events in Greenland.

As in Goujon et al. (2003), a limitation of our model is that the ice sheet thickness and lower boundary condition do not vary with time. Two parameters are imposed at the boundary between the ice and bedrock: the temperature and vertical speed. Basal temperature is inferred from borehole measurements. If it is colder than the melting temperature estimated as a function of hydrostatic pressure (equation 8 in Goujon et al., 2008), the basal vertical speed is nul. Otherwise, the melting temperature is used and the basal vertical speed (melting rate) needs to be specified in input.


*Supplementary Text S2:*


The major discrepancies between our model results with dust and $\delta^{15}N$ data with dust occur outside the range of calcium concentrations at modern sites. We hence illustrate here how the addition of simple thresholds on a minimum and maximum effect of calcium can strongly reduce the main discrepancies between our model results with dust and $\delta^{15}N$ data. We have thus adjusted the dust parameterization proposed by Freitag with two threshold ($Ca_{min}$ and $Ca_{max}$) such as:

- If $Ca < Ca_{min}$ : use the Freitag parameterization with $Ca = Ca_{min}$
- If $Ca > Ca_{max}$: use the Freitag parameterization with $Ca = Ca_{max}$
- If $Ca_{min} < Ca < Ca_{max}$, use the original Freitag parameterization

In this study, we have chosen values of 2ng/g and 50ng/g for respectively $Ca_{min}$ and $Ca_{max}$. Implementing threshold values on calcium (blue lines on the Figure S10) reduces the largest inconsistencies between model results and $\delta^{15}N$ data, in particular at NGRIP (through the threshold at high calcium concentration) and at WAIS (through the threshold at low calcium concentration).

# References

Arnaud, L., Lipenkov, V., Barnola, J.-M., Gay, M. and Duval, P.: Modelling of the densification of polar firn: characterization of the snow-firn transition, in Annals of Glaciology, vol. 26, pp. 39–44., 1998.

Arnaud, L., Barnola, J. M. and Duval, P.: Physical modeling of the densification of snow/firn and ice in, Phys. Ice Ore Rec., 26, 39–44, 2000.

Bazin, L., Landais, A., Lemieux-Dudon, B., Toyé Mahamadou Kele, H., Veres, D., Parrenin, F., Martinerie, P., Ritz, C., Capron, E., Lipenkov, V., Loutre, M. F., Raynaud, D., Vinther, B. M., Svensson, A., Rasmussen, S. O., Severi, M., Blunier, T., Leuenberger, M., Fisher, H., Masson-Delmotte, V., Chappellaz, J. and Wolff, E.: An optimized multi-proxy, multi-site Antarctic ice and gas orbital chronology (AICC2012): 120-800 ka, Clim. Past, 9(4), 1715–1731, 2013.

Buiron, D., Chappellaz, J., Stenni, B., Frezzotti, M., Baumgartner, M., Capron, E., Landais, A., Lemieux-Dudon, B., Masson-Delmotte, V., Montagnat, M., Parrenin, F. and Schilt, A.: TALDICE-1 age scale of the Talos Dome deep ice core, East Antarctica, Clim. Past, 7(1), 1–16, doi:10.5194/cp-7-1-2011, 2011.

Buizert, C., Martinerie, P., Petrenko, V. V., Severinghaus, J. P., Trudinger, C. M., Witrant, E., Rosen, J. L., Orsi, A. J., Rubino, M., Etheridge, D. M., Steele, L. P., Hogan, C., Laube, J. C., Sturges, W. T., Levchenko, V. A., Smith, A. M., Levin, I., Conway, T. J., Dlugokencky, E. J., Lang, P. M., Kawamura, K., Jenk, T. M., White, J. W. C., Sowers, T., Schwander, J. and Blunier, T.: Gas transport in firn: multiple-tracer characterisation and model intercomparison for NEEM, Northern Greenland, Atmospheric Chem. Phys., 12(9), 4259–4277, doi:10.5194/acp-12-4259-2012, 2012.

Buizert, C., Cuffey, K. M., Severinghaus, J. P., Baggenstos, D., Fudge, T. J., Steig, E. J., Markle, B. R., Winstrup, M., Rhodes, R. H., Brook, E. J., Sowers, T. A., Clow, G. D., Cheng, H., Edwards, R. L., Sigl, M., McConnell, J. R. and Taylor, K. C.: The WAIS Divide deep ice core WD2014 chronology-Part 1: Methane synchronization (68–31 ka BP) and the gas age–ice age difference, Clim. Past, 11(2), 153–173, doi:10.5194/cp-11-153-2015, 2015.

Butler, J. H., Battle, M., Bender, M. L., Montzka, S. A., Clarke, A. D., Saltzman, E. S., Sucher, C. M., Severinghaus, J. P. and Elkins, J. W.: A record of atmospheric halocarbons during the twentieth century from polar firn air, Nature, 399(6738), 749–755, 1999.

Capron, E., Landais, A., Buiron, D., Cauquoin, A., Chappellaz, J., Debret, M., Jouzel, J., Leuenberger, M., Martinerie, P., Masson-Delmotte, V., Mulvaney, R., Parrenin, F. and Prié, F.: Glacial–interglacial dynamics of Antarctic firn columns: comparison between simulations and ice core air-δ15N measurements, Clim. Past, 9(3), 983–999, doi:10.5194/cp-9-983-2013, 2013.

Clausen, H. B., Gundestrup, N. S., Johnsen, S. J., Bindschadler, R. and Zwally, J.: Glaciological investigations in the Crete area, central Greenland: A search for a new deep-drilling site, Ann Glaciol, 10, 10–15, 1988.

Cole-Dai, J., Ferris, D. G., Lanciki, A. L., Savarino, J., Thiemens, M. H. and McConnell, J. R.: Two likely stratospheric volcanic eruptions in the 1450s CE found in a bipolar, subannually dated 800 year ice core record, J. Geophys. Res. Atmospheres, 118(14), 7459–7466, 2013.

Cuffey, K. M. and Clow, G. D.: Temperature, accumulation, and ice sheet elevation in central Greenland through the last deglacial transition, J. Geophys. Res. Oceans, 102(C12), 26383–26396, 1997.

Cuffey, K. M. and Vimeux, F.: Covariation of carbon dioxide and temperature from the Vostok ice core after deuterium-excess correction, Nature, 523–526, 2001.

De Angelis, M., Steffensen, J. P., Legrand, M., Clausen, H. and Hammer, C.: Primary aerosol (sea salt and soil dust) deposited in Greenland ice during the last climatic cycle: Comparison with east Antarctic records, J. Geophys. Res. Oceans, 102(C12), 26681–26698, 1997.

Ding, M., Xiao, C., Yang, Y., Wang, Y., Li, C., Yuan, N., Shi, G., Sun, W. and Ming, J., "Re-assessment of recent (2008 2013) surface mass balance over Dome Argus, Antarctica," vol. 1, no. 2008 2013, pp. 1–8, 2016.

Etheridge, D. M. and Wookey, C. W.: Ice core drilling at a high accumulation area of Law Dome, Antarctica. 1987, Ice Core Drill., 10–14, 1988.

Ferris, D. G., Cole-Dai, J., Reyes, A. R. and Budner, D. M.: South Pole ice core record of explosive volcanic eruptions in the first and second millennia A.D. and evidence of a large eruption in the tropics around 535 A.D., J. Geophys. Res., 116(D17), doi:10.1029/2011JD015916, 2011.

Fischer, H., Fundel, F., Ruth, U., Twarloh, B., Wegner, A., Udisti, R., Becagli, S., Castellano, E., Morganti, A., Severi, M., Wolff, E., Littot, G., Röthlisberger, R., Mulvaney, R., Hutterli, M. A., Kaufmann, P., Federer, U., Lambert, F., Bigler, M., Hansson, M., Jonsell, U., de Angelis, M., Boutron, C., Siggaard-Andersen, M.-L., Steffensen, J. P., Barbante, C., Gaspari, V., Gabrielli, P. and Wagenbach, D.: Reconstruction of millennial changes in dust emission, transport and regional sea ice coverage using the deep EPICA ice cores from the Atlantic and Indian Ocean sector of Antarctica, Earth Planet. Sci. Lett., 260(1–2), 340–354, doi:10.1016/j.epsl.2007.06.014, 2007.

Fitzpatrick, J. J., Voigt, D. E., Fegyveresi, J. M., Stevens, N. T., Spencer, M. K., Cole-Dai, J., Alley, R. B., Jardine, G. E., Cravens, E. D., Wilen, L. A., Fudge, T. J. and McConnell, J. R.: Physical properties of the WAIS Divide ice core, J. Glaciol., 60(224), 1181–1198, doi:10.3189/2014JoG14J100, 2014.

Freitag, J., Kipfstuhl, S., Laepple, T. and Wilhelms, F.: Impurity-controlled densification: a new model for stratified polar firn, J. Glaciol., 59(218), 1163–1169, doi:10.3189/2013JoG13J042, 2013.

Fudge, T. J., Markle, B. R., Cuffey, K. M., Buizert, C., Taylor, K. C., Steig, E. J., Waddington, E. D., Conway, H. and Koutnik, M.: Variable relationship between accumulation and temperature in West Antarctica for the past 31,000 years: wdc temperature and accumulation, Geophys. Res. Lett., 43(8), 3795–3803, doi:10.1002/2016GL068356, 2016.

Gautier, E., Savarino, J., Erbland, J., Lanciki, A. and Possenti, P.: Variability of sulfate signal in ice core records based on five replicate cores, Clim. Past, 12(1), 103–113, doi:10.5194/cp-12-103-2016, 2016.

Gfeller, G., Fischer, H., Bigler, M., Schüpbach, S., Leuenberger, D. and Mini, O.: Representativeness and seasonality of major ion records derived from NEEM firn cores, The Cryosphere, 8(5), 1855–1870, doi:10.5194/tc-8-1855-2014, 2014.

Goujon, C., Barnola, J.-M. and Ritz, C.: Modeling the densification of polar firn including heat diffusion: Application to close-off characteristics and gas isotopic fractionation for Antarctica and Greenland sites, J. Geophys. Res. Atmospheres, 108(D24), 2003.

Gow, A. J.: Deep core studies of the accumulation and densification of snow at Byrd station and Little America V, Antarctica, CRREL., 1968.

Hörhold, M. W., Kipfstuhl, S., Wilhelms, F., Freitag, J. and Frenzel, A.: The densification of layered polar firn, J. Geophys. Res. Earth Surf., 116(F1), 2011.

Iizuka, Y., Horikawa, S., Sakurai, T., Johnson, S., Dahl-Jensen, D., Steffensen, J. P. and Hondoh, T.: A relationship between ion balance and the chemical compounds of salt inclusions found in the Greenland Ice Core Project and Dome Fuji ice cores, J. Geophys. Res., 113(D7), doi:10.1029/2007JD009018, 2008.

Jones, T. R., White, J. W. C. and Popp, T.: Siple Dome shallow ice cores: a study in coastal dome microclimatology, Clim. Past, 10(3), 1253–1267, doi:10.5194/cp-10-1253-2014, 2014.

Kindler, P., Guillevic, M., Baumgartner, M., Schwander, J., Landais, A., Leuenberger, M., Spahni, R., Capron, E. and Chappellaz, J.: Temperature reconstruction from 10 to 120 kyr b2k from the NGRIP ice core, Clim. Past, 10(2), 887–902, doi:10.5194/cp-10-887-2014, 2014.

Kipfstuhl, S., Faria, S. H., Azuma, N., Freitag, J., Hamann, I., Kaufmann, P., Miller, H., Weiler, K. and Wilhelms, F.: Evidence of dynamic recrystallization in polar firn, J. Geophys. Res., 114(B5), doi:10.1029/2008JB005583, 2009.

Kreutz, K. J., Mayewski, P. A., Twickler, M. S., Whitlow, S. I., White, J. W. C., Shuman, C. A., Raymond, C. F., Conway, H. and McConnell, J. R.: Seasonal variations of glaciochemical, isotopic and stratigraphic properties in Siple Dome (Antarctica) surface snow, Ann. Glaciol., 29(1), 38–44, 1999.

Kreutz, K. J., Mayewski, P. A., Meeker, L. D., Twickler, M. S. and Whitlow, S. I.: The effect of spatial and temporal accumulation rate variability in West Antarctica on soluble ion deposition, Geophys. Res. Lett., 27(16), 2517, 2000.

Lambert, F., Bigler, M., Steffensen, J. P., Hutterli, M. and Fischer, H.: Centennial mineral dust variability in high-resolution ice core data from Dome C, Antarctica, Clim. Past, 8(2), 609–623, doi:10.5194/cp-8-609-2012, 2012.

Langway, C. C. J.: Stratigraphic analysis of a deep ice core from Greenland, CRREL Res. Rep. 77, pp 130, 1967.

Leduc-Leballeur, M., Picard, G., Mialon, A., Arnaud, L., Lefebvre, E., Possenti, P. and Kerr, Y.: Modeling L-band brightness temperature at Dome C in Antarctica and comparison with SMOS observations, IEEE Trans. Geosci. Remote Sens., 53(7), 4022–4032, 2015.

Legrand, M. R., Lorius, C., Barkov, N. I. and Petrov, V. N.: Vostok (Antarctica) ice core: atmospheric chemistry changes over the last climatic cycle (160,000 years), Atmospheric Environ. 1967, 22(2), 317–331, 1988.

Mosley-Thompson, E., Thompson, L. G., Paskievitch, J. F., Pourchet, M., Gow, A. J., Davis, M. E. and Kleinman, J.: Recent increase in South Pole snow accumulation, Ann. Glaciol., 21(1), 131–138, 1995.

Narita, H. and Maeno, N.: II. Compiled Density Data from Cores Drilled at Mizuho Station (Appendix: Miscellaneous Compiled Data), Mem. Natl. Inst. Polar Res. Spec. Issue, 10, 136–158, 1978.

Ngrip community members: High-resolution record of Northern Hemisphere climate extending into the last interglacial period, Nature, 431(7005), 147–151, 2004.

Nishio, F., Fuji, Y. and Kusunoki, K.: Measured and computed temperature profiles at Mizuho station, East Antarctica, Sea Level Lee Clim. Change, 239–246, 1979.

Oerter, H., Graf, W., Meyer, H. and Wilhelms, F.: The EPICA ice core from Dronning Maud Land: first results from stable-isotope measurements, Ann. Glaciol., 39(1), 307–312, 2004.

Robin, G. de Q.: Profile data, Greenland region, Clim. Rec. Polar Ice Sheets Camb. Univ. Press Camb., 98–111, 1983.

Salamatin, A. N., Lipenkov, V. Y., Barnola, J. M., Hori, A., Duval, P. and Hondoh, T.: Snow/firn densification in polar ice sheets, Phys. Ice Core Rec. - II, 68(Supplement), 195–222, 2009.

Schüpbach, S., Federer, U., Kaufmann, P. R., Albani, S., Barbante, C., Stocker, T. F. and Fischer, H.: High-resolution mineral dust and sea ice proxy records from the Talos Dome ice core, Clim. Past, 9(6), 2789–2807, doi:10.5194/cp-9-2789-2013, 2013.

Schwander, J., Sowers, T., Barnola, J.-M., Blunier, T., Fuchs, A. and Malaizé, B.: Age scale of the air in the summit ice: Implication for glacial-interglacial temperature change, J. Geophys. Res. Atmospheres, 102(D16), 19483–19493, 1997.

Seierstad, I. K., Abbott, P. M., Bigler, M., Blunier, T., Bourne, A. J., Brook, E., Buchardt, S. L., Buizert, C., Clausen, H. B., Cook, E., Dahl-Jensen, D., Davies, S. M., Guillevic, M., Johnsen, S. J., Pedersen, D. S., Popp, T. J., Rasmussen, S. O., Severinghaus, J. P., Svensson, A. and Vinther, B. M.: Consistently dated records from the Greenland GRIP, GISP2 and NGRIP ice cores for the past 104 ka reveal regional millennial-scale δ18O gradients with possible Heinrich event imprint, Quat. Sci. Rev., 106, 29–46, doi:10.1016/j.quascirev.2014.10.032, 2014.

Shugui, H., Yuansheng, H., Cunde, X. L.Y. and Jiawen, R. E. N., "Recent accumulation rate at Dome A , Antarctica," vol. 52, no. 40576001, 2007.

Spencer, M. K., Alley, R. B. and Creyts, T. T.: Preliminary firn-densification model with 38-site dataset, J. Glaciol., 47(159), 671–676, 2001.

Steen-Larsen, H. C., Masson-Delmotte, V., Sjolte, J., Johnsen, S. J., Vinther, B. M., Bréon, F.-M., Clausen, H. B., Dahl-Jensen, D., Falourd, S., Fettweis, X., Gallée, H., Jouzel, J., Kageyama, M., Lerche, H., Minster, B., Picard, G., Punge, H. J., Risi, C., Salas, D., Schwander, J., Steffen, K., Sveinbjörnsdóttir, A. E., Svensson, A. and White, J.: Understanding the climatic signal in the water stable isotope records from the NEEM shallow firn/ice cores in northwest Greenland, J. Geophys. Res., 116(D6), doi:10.1029/2010JD014311, 2011.

Stenni, B., Proposito, M., Gragnani, R., Flora, O., Jouzel, J., Falourd, S. and Frezzotti, M.: Eight centuries of volcanic signal and climate change at Talos Dome (East Antarctica), J. Geophys. Res. Atmospheres, 107(D9), 2002.

Stenni, B., Masson-Delmotte, V., Selmo, E., Oerter, H., Meyer, H., Röthlisberger, R., Jouzel, J., Cattani, O., Falourd, S., Fischer, H., Hoffmann, G., Iacumin, P., Johnsen, S. J., Minster, B. and Udisti, R.: The deuterium excess records of EPICA Dome C and Dronning Maud Land ice cores (East Antarctica), Quat. Sci. Rev., 29(1–2), 146–159, doi:10.1016/j.quascirev.2009.10.009, 2010.

WAIS Divide Project Members: Onset of deglacial warming in West Antarctica driven by local orbital forcing, Nature, 500(7463), 440–444, doi:10.1038/nature12376, 2013.

Witrant, E., Martinerie, P., Hogan, C., Laube, J. C., Kawamura, K., Capron, E., Montzka, S. A., Dlugokencky, E. J., Etheridge, D., Blunier, T. and Sturges, W. T.: A new multi-gas constrained model of trace gas non-homogeneous transport in firn: evaluation and behaviour at eleven polar sites, Atmospheric Chem. Phys., 12(23), 11465–11483, doi:10.5194/acp-12-11465-2012, 2012.

Xiao, C., I. Allison, Y. Li, Hou, S., Dreyfus, G. B., Barnola, J.-M., Jiawen, R. E. N., Lingen, B., Shenkai, Z., and Kameda, T., "Surface characteristics at Dome A, Antarctica: first measurements and a guide to future ice-coring sites," *Ann. Glaciol.*, pp. 82–87, 2008.